Inferring Fitness Landscapes and Selection on Phenotypic States from Single-Cell Genealogical Data

Takashi Nozoe[1], Edo Kussell[2], Yuichi Wakamoto[1*]

1 Graduate School of Arts and Sciences, University of Tokyo, Tokyo, Japan
2 Center for Genomics and Systems Biology, Department of Biology, Department of Physics, New York University,New York, New York

* cwaka@mail.ecc.u-tokyo.ac.jp

Abstract

Recent advances in single-cell time-lapse microscopy have revealed non-genetic heterogeneity and temporal fluctuations of cellular phenotypes. While different phenotypic traits such as abundance of growth-related proteins in single cells may have differential effects on the reproductive success of cells, rigorous experimental quantification of this process has remained elusive due to the complexity of single cell physiology within the context of a proliferating population. We introduce and apply a practical empirical method to quantify the fitness landscapes of arbitrary phenotypic traits, using genealogical data in the form of population lineage trees which can include phenotypic data of various kinds. Our inference methodology for fitness landscapes determines how reproductivity is correlated to cellular phenotypes, and provides a natural generalization of bulk growth rate measures for single-cell histories. Using this technique, we quantify the strength of selection acting on different cellular phenotypic traits within populations, which allows us to determine whether a population responds to environmental perturbations by physiological changes in single cells, through population-level selection, or by a mixture of single-cell and population-level processes. By applying these methods to single-cell time-lapse data of growing bacterial populations that express a resistance-conferring protein under antibiotic stress, we show that selection acts on the resistance protein's production rate rather than on its concentration. Our work provides a unified and practical framework for quantitative measurements of fitness landscapes and selection strength for any statistical quantities definable on lineages, and thus elucidates the adaptive significance of phenotypic states in time series data. The method is applicable in diverse fields, from single cell biology to stem cell differentiation and viral evolution.

Introduction

Selection is a process in which the interaction of organisms with their environment determines which types of individuals thrive and proliferate more than others. Genetic information encoded in the genome is a primary determinant of reproductivity, but epigenetic and fluctuating phenotypic traits can also strongly influence selection [1–4]. Recent single-cell measurements revealed the existence of phenotypic heterogeneity within clonal populations, including cases in which heterogeneity has been shown to have a clear functional role [5, 6] such as bacterial persistence [7, 8], infection [9], and competence and sporulation [10]. Quantifying reproductivity of phenotypic traits and revealing how strongly selection acts within a

clonal population are thus of crucial importance for understanding the biological significance of phenotypic heterogeneity.

To experimentally evaluate reproductivity of a unicellular organism, one usually measures bulk growth rate (Malthusian parameter [11]) of a cellular population in batch or using a competition assay between a genotype of interest and a reference genotype [12]. These methods are only valid when the time-scale of genotypic changes is sufficiently long compared with that of the measurements. However, the time-scale of phenotypic changes is often comparable to cellular generation time, and only in certain cases is it orders of magnitude longer, e.g. when a phenotypic state is stabilized by specific epigenetic and/or positive-feedback regulations. As a result, bulk population growth rates of sub-populations fractionated based on initial phenotypic traits, e.g. by fluorescence-activated cell sorting, do not necessarily represent reproductivity of initial phenotypic traits because phenotypic traits are diversified rapidly by complex dynamical processes that occur during measurements. An alternative approach is necessary to measure reproductivity for heterogeneous and fluctuating cellular phenotypes.

Using time-lapse microscopy and fluorescent reporters, it has become possible to follow full individual cell histories recording all division events and instantaneous expression levels of reporters within cellular populations [8, 13–18]. Several theoretical studies have demonstrated the utility of history-based analysis of growing populations, regarding individual histories rather than single cells as the basic replicating entity [19–21]. For example, Leibler and Kussell introduced a time-integrated instantaneous reproduction rate, termed *historical fitness* [19], and defined a measure of selection using the response of mean historical fitness over all histories within a population. However, empirically determining the instantaneous reproduction rate of an individual cell can be difficult in general, e.g. due to the fact that cell size, age, elongation rate, and division timing are a subset of possible observables all of which contribute to reproduction. Evaluating the fitness value of a certain phenotypic trait such as expression level of a specific gene results in additional complications.

To address these difficulties, we introduce an empirically measurable quantity associated with phenotypic states, which we call the phenotypic *fitness landscape*. This quantity, which reports how cellular reproductivity is correlated with phenotypic states, extends the definition of historical fitness so that it becomes meaningful in a general setting without requiring any assumptions. Our approach allows one to assign a fitness value to any statistical quantities observed over cellular lineages, and to evaluate the selection strength acting on different phenotypic states. To formulate our framework, we leverage a fundamental property of selection processes: the *retrospective probability* of observing a certain phenotypic trait value by moving backward in time from the present to the ancestral parts of a lineage is different from its counterpart, the *chronological probability* to observe the trait value moving forward in time along a lineage as individuals grow and divide. We show that these two probabilities can be evaluated directly using single-cell lineage tree data, leading to natural definitions of the fitness landscape and selection strength. We apply this framework to analyze proliferation processes of simulated and experimental cellular populations, demonstrating the utility of our measures to reveal phenotype dependent fitness and its response to environmental change.

Results

Retrospective and chronological probabilities for single cell lineages

We consider a binary division process as depicted in Fig 1, where t_0, t_1 are the start and end times of a lineage tree, and we define $\tau = t_1 - t_0$ as the duration of observation. To illustrate our view of lineage statistics, we first consider a single fixed lineage tree denoted by $\mathcal{T}$ derived from a single ancestor cell (Fig 1A). Let $N(t, \mathcal{T})$ be the number of cells in the tree $\mathcal{T}$ at time t and we label and distinguish each lineage by $i = 1, 2, ..., N(t_1, \mathcal{T})$. We consider two different ways of randomly sampling single-cell lineages on the tree. We could sample each lineage with equal weight, where the probability of choosing lineage i is $\pi_i^{\mathrm{rs}} = 1/N(t_1, \mathcal{T})$, which we call the *retrospective probability* because it corresponds to the probability that the past history of the last cell on lineage i is chosen. Alternatively, letting D_i be the number of cell divisions on lineage i, we could sample lineage i with probability $\pi_i^{\mathrm{cl}} = 2^{-D_i}$, which we call the *chronological probability* because it is the probability that lineage i is chosen by descending the tree from the ancestor cell at t_0 randomly at each branch point with equal probability 1/2. The probability distribution π_i^{cl} is determined solely by the number of divisions on lineage i, being unaffected by the reproductive performance of the other lineages. In contrast, π_i^{rs} strongly depends on the reproductive performance on the other lineages, which enters into the total number of cell lineages.

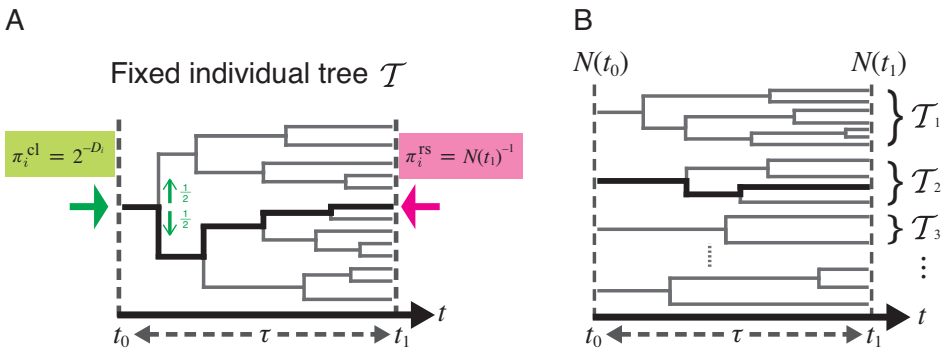

Fig 1. Chronological and retrospective probabilities of single-cell lineages. A. Chronological and retrospective probabilities on a fixed tree. Here we consider a representative fixed lineage tree $\mathcal{T}$ spanning from time t_0 to $t_1 = t_0 + \tau$. The number of cells in this tree at t_1 is $N(t_1) = 13$ cells, and each of these cells distinguishes a unique lineage (e.g. the thick black line in the tree). π_i^{cl} is the probability that a cell lineage i ($i = 1, 2, \cdots, N(t_1)$) is chosen by descending the tree from t_0 to t_1 (green arrow). At every division point, we randomly select one daughter cell's lineage with the probability of 1/2 (light green arrows). The probability that we choose lineage i in this manner is $\pi_i^{\mathrm{cl}} = 2^{-D_i}$, where D_i is the number of cell divisions on lineage i. π_i^{rs} is the probability of choosing cell lineage i among $N(t_1)$ lineages with equal weight (pink arrow). Thus, $\pi_i^{\mathrm{rs}} = N(t_1)^{-1}$. We call π_i^{cl} and π_i^{rs} the chronological probability and retrospective probability, respectively, based on the time directions of the green and pink arrows. For the cell lineage indicated by the thick line, $\pi_i^{\mathrm{rs}} = 1/13 > \pi_i^{\mathrm{cl}} = 2^{-4} = 1/16$. **B.** General case with a large collection of lineage trees.

Lineage fitness and fitness landscape on a phenotypic trait

Next, we consider the set of lineages within a large collection of independent trees initiated from a large number of progenitor cells $N(t_0) \gg 1$ (Fig 1B). For each lineage, we record a phenotypic trait x and the number of divisions D, where x can be any random variable representing a phenotypic trait of a single cell lineage, e.g. a time-averaged gene expression level, average cell length, number of divisions D, or any variety of other possibilities. We consider the joint statistics of D and x across all possible trees, letting $n(D, x, \mathcal{T})$ denote the number of lineages with values D and x within tree $\mathcal{T}$, and we denote the sum of this quantity over trees as $n(D, x)$. The total number of lineages observed across all trees, $N(t_1)$, is given by summing $n(D, x)$ over D and x. In analogy with the single tree quantities, we define the retrospective probability of choosing a lineage with D and x as

$$P^{\mathrm{rs}}(D, x) \equiv \frac{n(D, x)}{N(t_1)}, \tag{1}$$

and the chronological probability as

$$P^{\mathrm{cl}}(D, x) \equiv \frac{2^{-D}}{N(t_0)} n(D, x) \ . \tag{2}$$

Defining Λ to be the population growth rate,

$$\Lambda \equiv \frac{1}{\tau} \ln \frac{N(t_1)}{N(t_0)} \ , \tag{3}$$

we obtain using equations 1 and 2 the relation

$$P^{\mathrm{rs}}\left(D, x\right) = e^{D \ln 2 - \tau \Lambda} P^{\mathrm{cl}}\left(D, x\right) \ . \tag{4}$$

We see from Eq. 4 that $\tilde{h}(D) \equiv \tau^{-1} D \ln 2$ is the natural measure of fitness for a lineage, since lineages for which this quantity is greater than Λ will be exponentially over-represented in retrospective probability relative to chronological probability.

We now measure how quickly the number of lineages with a given phenotype x grow between times t_0 and t_1 according to their chronological and retrospective probabilities. We denote by $P^{\mathrm{rs}}(x) \equiv \sum_D P^{\mathrm{rs}}(D, x)$ and $P^{\mathrm{cl}}(x) \equiv \sum_D P^{\mathrm{cl}}(D, x)$ the retrospective and chronological marginal probability distributions of x. We define the phenotypic *fitness landscape* $h(x)$ as

$$h\left(x\right) \equiv \frac{1}{\tau} \ln \frac{N(t_1) P^{\mathrm{rs}}(x)}{N(t_0) P^{\mathrm{cl}}(x)} = \Lambda + \frac{1}{\tau} \ln \frac{P^{\mathrm{rs}}(x)}{P^{\mathrm{cl}}(x)} \ , \tag{5}$$

noting that $N(t_0) P^{\mathrm{cl}}(x)$ and $N(t_1) P^{\mathrm{rs}}(x)$ are the effective numbers of cell lineages with a phenotypic trait x from the chronological and retrospective perspectives, respectively. We can rewrite Eq. 5 as

$$P^{\mathrm{rs}}\left(x\right) = e^{\tau(h(x) - \Lambda)} P^{\mathrm{cl}}\left(x\right), \tag{6}$$

which shows that if $h(x)$ is greater than Λ the phenotypic state x will be exponentially over-represented in retrospective relative to chronological probability. Thus, $h(x)$ provides a natural extension of fitness for lineage-based phenotypic traits.

Measuring the strength of phenotypic selection

Specific states of the phenotypic trait x can be selected if x and D are correlated. In general, the strength of this correlation could differ significantly among different phenotypes. In the conventional framework of natural selection known as Fisher's fundamental theorem, selection strength is measured by the gain of mean fitness due to the change of probability distribution of a phenotype [11]. Inspired by this idea, we define the strength of selection acting on phenotypic trait x as

$$S\left[x\right] \equiv \langle h(x)\rangle^{\mathrm{rs}} - \langle h(x)\rangle^{\mathrm{cl}}, \tag{7}$$

where $\langle h(x)\rangle^{\mathrm{rs}} = \sum_x h(x)P^{\mathrm{rs}}(x)$ and $\langle h(x)\rangle^{\mathrm{cl}} = \sum_x h(x)P^{\mathrm{cl}}(x)$ are the mean fitness in retrospective and chronological perspectives, respectively.

This simple measure of selection strength has rich underpinnings. First, $S[x]$ is also a measure of fitness variation on the landscape $h(x)$ because

$$S\left[x\right] \approx \tau \mathrm{Cov}\left[\tilde{h}(D), h(x)\right] \approx \tau \mathrm{Var}\left[h(x)\right] \ , \tag{8}$$

where the variance and covariance can equivalently be taken over either chronological or retrospective distributions, and the approximation is accurate to the order of second cumulants of $\tilde{h}(D)$ and $h(x)$ (see *Supporting Information*). Secondly, $S[x]$ also represents the statistical deviation between the probability distributions $P^{\mathrm{cl}}(x)$ and $P^{\mathrm{rs}}(x)$ because

$$S[x] = \frac{1}{\tau} J\left[P^{\mathrm{cl}}(x), P^{\mathrm{rs}}(x)\right], \tag{9}$$

where $J\left[p(x), q(x)\right] \equiv \sum_x \left(p(x) - q(x)\right) \ln \frac{p(x)}{q(x)}$ is the Jeffereys divergence [22–24] (see *Supporting Information*). The deviation between $P^{\mathrm{rs}}(x)$ and $P^{\mathrm{cl}}(x)$ is thus directly linked to the selection strength on x.

From the properties of Jeffreys divergence, we can prove that

$$0 \leq S[x] \leq S[D]. \tag{10}$$

Selection strengths of any phenotypic states are therefore bounded by that of D. As described in *Supporting Information*, $S[x]$ can be interpreted as an amount of information representing to what extent variation of D can be explained by phenotype x. Therefore, when $S[x]$ is large, phenotype x is strongly correlated with lineage fitness. In fact, we can prove that $S_{\mathrm{rel}}[x] \equiv \frac{S[x]}{S[D]}$ is approximately equal to the squared correlation coefficient between $\tilde{h}(D)$ and $h(x)$ to the order of second cumulants (Eq. S55).

Decomposition of fitness response to environmental change

We now introduce an explicit dependence of all quantities on an environment variable $\mathcal{E}$, and using this notation Eq.7 becomes

$$S[x](\mathcal{E}) \equiv \langle h(x;\mathcal{E})\rangle^{\mathrm{rs},\mathcal{E}} - \langle h(x;\mathcal{E})\rangle^{\mathrm{cl},\mathcal{E}}. \tag{11}$$

Let us denote the changes of mean fitness and selection strength due to an environmental shift from $\mathcal{E}_1$ to $\mathcal{E}_2$ as $\Delta\langle h(x)\rangle^{\mathrm{cl}}$, $\Delta\langle h(x)\rangle^{\mathrm{rs}}$ and $\Delta S[x]$. Then

$$\Delta\langle h(x)\rangle^{\mathrm{rs}} = \Delta\langle h(x)\rangle^{\mathrm{cl}} + \Delta S[x]. \tag{12}$$

$\Delta\langle h(x)\rangle^{\mathrm{rs}}$ represents the response of mean fitness in retrospective histories due to the change of the environments. Eq. 12 indicates that this term can be decomposed into two terms: $\Delta\langle h(x)\rangle^{\mathrm{cl}}$, which represents the intrinsic response to the environmental change; and $\Delta S[x]$, the change of selection strength. Thus, this framework allows us to distinguish and evaluate the contributions of individual response and selection to the total change of retrospective mean fitness.

In *Supporting Information*, we apply the above framework to several analytically tractable models, and directly calculate fitness landscape and selection strength in each model. We also show the examples of fitness decomposition in *Supporting Information*.

Simulation

To demonstrate the utility of our lineage-based analysis, we first applied it to simulation data of a cell proliferation model. In this model, we consider a population in which cells divide according to division probability $f(y_t)\Delta t$, where Δt is time increment, and y_t is a variable that represents an instantaneous state of a certain phenotype at time t. For example, y_t can be an intracellular concentration of some protein. In the simulation, we evolved y_t assuming that $\ln y_t$ follows the Ornstein-Uhlenbeck process so that the stationary distribution of y_t in chronological cell histories follows the log-normal distribution with mean 1 and standard deviation 0.3. We set $f(y)$ to be a Hill function, $f(y) = \frac{y^n}{1+y^n} f_{\max}$, where n is the Hill coefficient, and $f_{\max}$ is the maximum division rate. We fixed $f_{\max} = 1.2\ \mathrm{h}^{-1}$ and ran the simulation under different values of n. The initial state of a cell lineage at t_0 was randomly sampled from the stationary log-normal distribution. In each condition, we repeated the simulation 100 times, i.e. $N(t_0) = 100$, which is a realistic sample size of single-cell time-lapse experiments. To calculate fitness landscape and selection strength, we used the lineage tree data between $t_0 = 0$ min and $t_1 = 250$ min (thus $\tau = 250$ min). Additional details of simulation are described in Section Materials and Methods.

As a phenotypic trait of cell lineages, we chose the time-average of y_t; i.e.

$$x = \overline{y}_\tau \equiv \frac{1}{\tau}\int_{t_0}^{t_1} y_t dt. \tag{13}$$

The result shows that the fitness landscape $h(\overline{y}_\tau)$ calculated from the simulated lineage trees and the time-series of y_t retrieves $f(y)$ in a relatively good precision despite the non-linearity of $f(y)$ (Fig 2A and Fig S1A and S1B in *Supporting Information*). The chronological mean fitness $\langle h(\overline{y}_\tau)\rangle^{\mathrm{cl}}$ is unchanged by the change of n, but the retrospective mean fitness $\langle h(\overline{y}_\tau)\rangle^{\mathrm{rs}}$ increases significantly with n (Fig 2B). As a result, selection strength $S[\overline{y}_\tau] = \langle h(\overline{y}_\tau)\rangle^{\mathrm{rs}} - \langle h(\overline{y}_\tau)\rangle^{\mathrm{cl}}$ as well as relative selection strength $S_{\mathrm{rel}}[\overline{y}_\tau]$ increase with n as expected from the fact that larger n introduces greater fitness variation (Fig 2B and C). Reducing the autocorrelation time of y_t decreases selection strength (Fig S1C in *Supporting Information*), since faster fluctuations of the phenotype decrease the variation of the time average, $\overline{y}_\tau$. In this case, $h(\overline{y}_\tau)$ deviates slightly from $f(y)$ when the non-linearity is strong ($n = 10$, Fig S1A and S1B in *Supporting Information*), which results from the fact that the time-average of $f(y_t)$ is not equivalent to $f(\bar{y}_\tau)$, an effect that becomes pronounced when n is large. These results show that our lineage-based analysis allows us to probe fitness and selection strength of heterogeneous cellular phenotypes from realistic sample sizes of single-cell lineage trees.

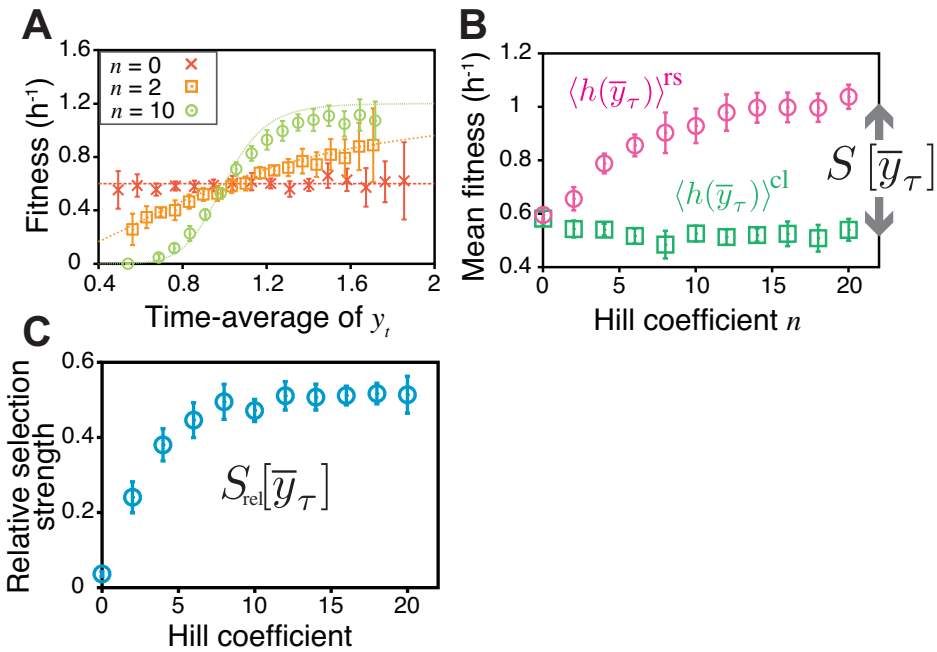

Fig 2. Quantifying fitness landscape and selection strength for the simulation data of clonal cell proliferation. A. Fitness landscapes. We produced the datasets of clonal cell proliferation by simulation, in which we assumed that cells stochastically change phenotypic state y and divide in a phenotype-dependent manner with the division rate $f(y) = \frac{y^n}{1+y^n} f_{\max}$. We calculated fitness landscapes $h(\bar{y})$ from the simulation data for the conditions of $n = 0$, 2, and 10. In all the conditions, $h(\bar{y})$ (points) recovered the assigned phenotype-dependent division rate $f(y)$ (broken curves) with good precision. The points and the error bars represent means and standard deviations of results from 10 independent simulations (same in B and C). **B.** Dependence of mean fitness $\langle h(\bar{y}_\tau)\rangle^{\mathrm{cl}}$ and $\langle h(\bar{y}_\tau)\rangle^{\mathrm{rs}}$ on Hill coefficient. Strengthening phenotype-dependence of fitness by increasing the Hill coefficient in $f(y)$ caused $\langle h(\bar{y}_\tau)\rangle^{\mathrm{rs}}$ (magenta circles) to be greater than $\langle h(\bar{y}_\tau)\rangle^{\mathrm{cl}}$ (green squares). In our definition, selection strength for phenotype $\bar{y}_\tau$ is given by $\langle h(\bar{y}_\tau)\rangle^{\mathrm{rs}} - \langle h(\bar{y}_\tau)\rangle^{\mathrm{cl}}$ (Eq. 7), thus the deviation directly indicates the existence of selection acting on phenotype $\bar{y}_\tau$. **C.** Dependence of relative selection strength $S_{\mathrm{rel}}[\bar{y}_\tau] = S[\bar{y}_\tau]/S[D]$ on Hill coefficient.

Single-cell time-lapse experiment

Next we apply this analytical framework to real single-cell time-lapse data of *E. coli*, which expresses an antibiotic resistance gene sm^R [25] and a fluorescent reporter *venus-yfp* [26] from a low copy plasmid under the control of a common promoter PLlacO-1 [27] (Fig 3A). The Sm^{R} protein confers the resistance to a ribosome-targetting antibiotic drug, streptomycin, by direct inactivation [28, 29]. We conducted fluorescent time-lapse measurements of cells proliferating on agarose pads that contain either no drug (Sm−) or a sub-inhibitory concentration of streptomycin (Sm+) (200 µg/ml; minimum inhibitory concentration (MIC) is 1000 µg/ml, Fig 3B) (Fig 3C). We extracted the information of lineage trees (Fig 3D) along with time-series of cell size $v(t)$ and of fluorescence intensity $c(t)$ (Fig 3E). Since $c(t)$ is a proxy for protein concentration in a cell, $c(t)v(t)$ can be regarded as the quantity that scales with the

total amount of protein in a cell. Based on these quantities, we analyzed three different time-averaged phenotypes along a single-cell lineage: elongation rate $\bar{\lambda}_\tau$, protein production rate $\bar{p}_\tau$, and protein concentration $\bar{c}_\tau$, which are defined as

$$\bar{\lambda}_\tau \equiv \frac{1}{\tau}\int_{t_0}^{t_1} \frac{d}{dt} \ln v(t) dt, \tag{14}$$

$$\bar{p}_\tau \equiv \frac{1}{\tau}\int_{t_0}^{t_1} \frac{1}{v(t)} \frac{d}{dt} \left[c(t)v(t)\right] dt, \tag{15}$$

$$\bar{c}_\tau \equiv \frac{1}{\tau}\int_{t_0}^{t_1} c(t) dt \ . \tag{16}$$

We calculated these phenotypic quantities for all the lineages spanning from t_0 to t_1, and obtained the chronological probability distribution $P^{\mathrm{cl}}(\cdot)$, fitness landscape $h(\cdot)$, and selection strength $S[\cdot]$ of these phenotypes.

Population growth kinetics revealed that the growth rate difference between Sm− and Sm+ conditions was small and became noticeable only after $t = 200$ min (Fig 4A). Therefore, we focused on the time window between $t_0 = 200$ min and $t_1 = 400$ min (see Fig S2 in *Supporting Information* for the results when $t_0 = 0$ min and $t_1 = 200$ min). The population growth rates during this period were 0.45±0.01 h^{-1} for Sm− and 0.39±0.01 h^{-1} for Sm+, respectively ($p < 0.05$) (Fig 4B). Consistently, the mean of lineage fitness in the chronological perspective $\langle \tilde{h}(D) \rangle^{\mathrm{cl}}$ in Sm+ condition was 0.35±0.01 h^{-1}, which is smaller than that in Sm− condition, 0.41±0.01 h^{-1} ($p < 0.05$) (Fig 4C). Despite the decrease in the mean lineage fitness, we did not detect the difference in intra-population lineage heterogeneity measured by maximum selection strength $S[D]$ ($p = 0.5$) (Fig 4D).

The three lineage phenotypes had distinct characteristics in their response to the drug (Fig 4E-I). The fitness landscapes of elongation rate were nearly identical between Sm− and Sm+ conditions, and increased approximately linearly with $\bar{\lambda}_\tau$ (Fig 4E). This agrees with the natural assumption that fast elongation should lead to proportionately high division rate. The chronological distribution $P^{\mathrm{cl}}(\bar{\lambda}_\tau)$ shifted to the left in Sm+ condition (Fig 4E), which is also consistent with the fact that $\langle \tilde{h}(D) \rangle^{\mathrm{cl}}$ is slightly lower in Sm+ condition. Nevertheless, we did not detect the difference in selection strength $S[\bar{\lambda}_\tau]$ (Fig 4H). These results confirm that $\bar{\lambda}_\tau$ behaves coherently with D under those conditions.

The fitness landscape of protein production rate were likewise nearly identical between Sm+ and Sm− conditions (Fig 4F). The landscape is a more saturating function rather than linear with the kink around 0.5 FL unit/h. The fact that $h(\bar{p}_\tau)$ is an increasing function even in the absence of the drug is presumably because overall cellular metabolism couples to all production rates and cells growing faster generally have higher production rates in most genes. The chronological distribution $P^{\mathrm{cl}}(\bar{p}_\tau)$ shifted significantly toward the left in Sm+ condition. Interestingly, we detected an increased selection strength $S[\bar{p}_\tau]$ in Sm+ condition (1.7×10^{-2} h^{-1}) compared with that in Sm− condition (0.5×10^{-2} h^{-1}, $p < 0.05$) (Fig 4H). This indicates that the heterogeneity in Sm^{R} production rate begins to play a role in causing fitness heterogeneity within a population exposed to the drug. This change in the selection strength largely comes from the shift of the chronological distribution $P^{\mathrm{cl}}(\bar{p}_\tau)$: A large portion of the probability distribution resides in the platau region of the fitness landscape in Sm− condition, whereas its shift in Sm+ condition causes a significant overlap with the linear region, resulting in a larger fitness heterogeneity in the phenotypic space of $\bar{p}_\tau$.

The fitness landscapes of protein concentration decrease linearly with $\bar{c}_\tau$ in both Sm+ and Sm− conditions; protein expression levels and fitness are thus anti-correlated (Fig 4G). Surprisingly, we did not detect any advantages of high expression level even in the presence of the drug (Fig 4G). The chronological distribution $P^{\mathrm{cl}}(\bar{c}_\tau)$ and selection strength $S[\bar{c}_\tau]$ were nearly identical between the two conditions (Fig 4G and 4H). This indicates that, unlike production rate $\bar{p}_\tau$, the heterogeneity in Sm^{R} expression level per se does not induce any additional selection even if the drug is added at this concentration. The results therefore suggest that the protein production rate of Sm^{R} is a more responsive phenotype to selection than protein expression level. The response characteristics of selection strength are unchanged even if the relative selection strengths were compared between the two conditions (Fig 4I).

Applying fitness decomposition in Eq. 12 to the experimental data revealed that the changes of mean fitness in retrospective perspective due to the environmental change from Sm− to Sm+ ($\Delta\langle h(x)\rangle^{\mathrm{rs}}$) mostly came from the changes in $\Delta\langle h(x)\rangle^{\mathrm{cl}}$, not from the changes in selection strengths $\Delta S[x]$, for all the phenotypes (Table 1). Therefore, the contribution of $\Delta S[x]$ to $\Delta\langle h(x)\rangle^{\mathrm{rs}}$ were marginal at least in the environmental difference used in this study.

Table 1. Contributions of individual cells' response $\Delta\langle h(x)\rangle^{\mathrm{cl}}$ and change of selection strength $\Delta S[x]$ to fitness gain $\langle h(x)\rangle^{\mathrm{rs}}$ for the environmental change from Sm− to Sm+.

	Division D	Elongation $\bar{\lambda}_\tau$	Protein production $\bar{p}_\tau$	Protein concentration $\bar{c}_\tau$
$\Delta\langle h(x)\rangle^{\mathrm{rs}}$	-0.05 ± 0.02	-0.05 ± 0.02	-0.05 ± 0.02	-0.06 ± 0.02
$\Delta\langle h(x)\rangle^{\mathrm{cl}}$	-0.06 ± 0.02	-0.06 ± 0.02	-0.06 ± 0.02	-0.06 ± 0.02
$\Delta S[x]$	0.005 ± 0.009	0.007 ± 0.008	0.012 ± 0.006	0.000 ± 0.004

We found that the relative selection strengths of $x = \bar{\lambda}_\tau$, $\bar{p}_\tau$, and $\bar{c}_\tau$ were approximately equal to the squared correlation coefficients between $\tilde{h}(D)$ and $h(x)$ evaluated by both chronological and retrospective probabilities (Fig 4J). This validates the simple interpretation that $S_{\mathrm{rel}}[x]$ represents the correlation between $\tilde{h}(D)$ and $h(x)$, though the small differences of the squared correlation coefficients between the chronological and retrospective probabilities suggest the contribution of higher-order cumulants (*Supporting Information*).

Discussion

In this report, we have presented a method to quantify fitness differences and selection strength for heterogeneous phenotypic states of individual cells within a population. Our framework shares a basic idea with the method for measuring selection strength developed in evolutionary biology in that we evaluate phenotype-dependent fitness [30–32]. The important differences are: (1) we treated a single-cell lineage or history as the unit of proliferation; (2) we assigned the statistical weight 2^D to each cell history as proposed in [20]; and (3) we treated natural logarithm of the expected statistical weight conditioned on a phenotypic state of cell history as the measure of fitness.

An important advantage of history-based formulation of fitness landscape and selection strength is that it is applicable even to cellular phenotypes that fluctuate in time like gene expression levels in single cells. Indeed, we demonstrated by simulation that the pre-assigned fitness landscape was retrievable from the single-cell lineage trees and the associated dynamics of cellular phenotypic states despite the stochastic transition of the states. Though a number

of single cell studies have suggested the functional roles of phenotypic fluctuation in a genetically uniform cell population [5,6], our framework provides the first procedure for the rigorous quantification of the fitness values of such fluctuating cellular states. In this framework, we can use any statistical quantities that are measurable on cell lineages as the 'phenotype'. Although we exclusively evaluated the time-averages of cellular phenotypes along cell lineages in the analysis, the other statistical quantities such as variance and coefficient of variation can be also evaluated as lineage phenotypes, which might reveal e.g. the fitness value of "noisiness" of gene expression level. Conversely, the flexibility imposes a technical challenge to select a suitable quantity that correctly reports cellular functions. We emphasize that the fitness landscapes and selection strengths quantified in this study report only correlation between the lineage phenotypes and cell division, not causality. To address causality, one must carefully choose appropriate lineage phenotypes that take detailed time-series of phenotypic states into account.

We applied our method to real clonal proliferation processes of *E. coli*, and quantified the fitness landscape and the selection strength for different phenotypes with and without an antibiotic drug. An interesting observation was that the selection strength for time-averaged protein concentration of Sm^{R} was indistinguishable between the two environments, whereas that for time-averaged protein production rate increased significantly by drug exposure. This result suggests that, at least in the drug exposure condition used in this experiment, the role of the resistance gene in individual cells is better represented by its production rate than its intracellular concentration. Since our study is limited to a single drug at a single concentration, extending the measurements to broad conditions is an important future subject for understanding how gene expression influences cellular fitness.

It is important to note that the conventional genetic perturbation methods such as gene knock-out, overexpression, and gene suppression only associate a population-level gene expression state with population fitness; they are unable to report whether different expression states of single cells in the same population are correlated to their fitness. Our new analytical framework, however, allows us to reveal the impact of different expression levels and dynamics to cellular fitness without modifying population-level expression states, and might open up a new field in genetics that connects different expression states to cellular fitness without applying the genetic perturbation.

The application of this method is not restricted to the analysis of clonal proliferation in unicellular organisms. An important application would be in the analysis of embryogenesis and stem cell differentiation of multicellular organisms, in which cellular reproduction rates diversify among the branches of lineage trees as the differentiation process goes forward [33]. Recently, large-scale cell lineage trees along with detailed quantitative information on cellular phenotypes (gene expression, cell position, movement, etc.) have been available [17,18,34,35]. Quantifying fitness and selection strength for different phenotypes at the single-cell level in differentiation processes might reveal key phenotypic steps and events leading to cell fate diversification. Additionally, fruitful applications may be found in the analysis of evolutionary lineages in viral populations, such as influenza [36] and HIV [37], where lineage trees have been obtained using temporal sequencing data. Quantifying the strength of selection on viral traits, such as antigenic determinants, and inferring their fitness landscape is an important challenge in the field [38–40] which the method presented here could address. The application of this new lineage analysis tool to broader biological contexts may unravel the roles of phenotypic heterogeneity in diverse cellular and evolutionary phenomena.

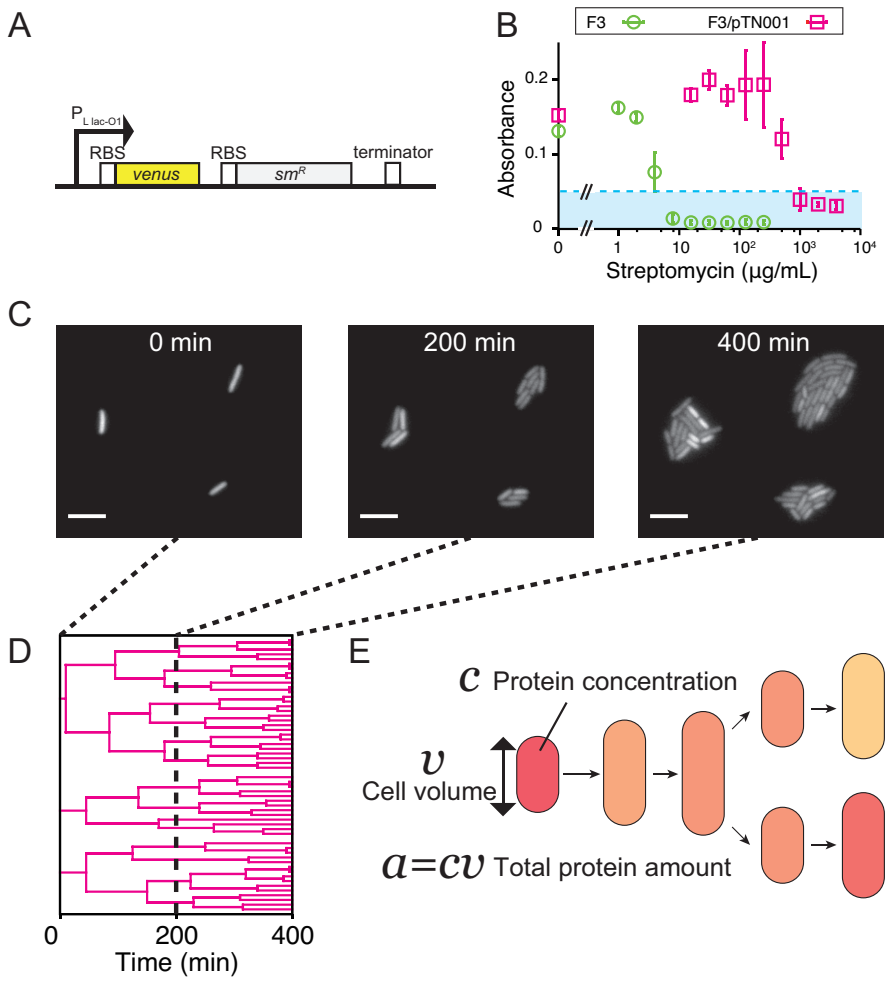

Fig 3. Single-cell time-lapse measurements. A Fluorescent reporter and drug resistance genes transcribed from common promoter. We used an *E. coli* strain F3/pTN001 (W3110 derivative), which expresses a fluorescent protein Venus-YFP and streptomycin resistance-conferring protein Sm^R under the control of PLlac-O1 promoter from a low copy plasmid pTN001 (pSC101 ori). Ribosomal binding sites are present in front of the start codons of both structural genes, thus proteins are translated separately. We analyzed the data assuming that production rate and protein amount of Sm^R are strongly correlated with those of Venus-YFP. **B** MICs of streptomycin for F3 and F3/pTN001. Absorbance at 595 nm of cell cultures of F3 or F3/pTN001 at different concentrations of streptomycin was measured after 20-hour incubation with shaking at 37°C. The average of three replicates are plotted with the standard deviation for each condition of streptomycin concentration. We determined MICs by the minimum concentration above which the absorbance of cell culture remains below 0.05 (cyan region): 8 μg/mL for F3 (green) and 1000 μg/mL for F3/pTN001 (magenta). **C** Representative time-lapse fluorescent images in Sm+ condition. Images were acquired every five minutes. Approximately 100 microcolonies were simultaneously observed in each time-lapse experiment. Scale bars, 5 μm. **D** Cell lineage trees for the three microcolonies in (B). **E** Quantities obtained from time-lapse images. We extracted the time-series of cell volume v, protein concentration (mean fluorescence intensity on cell area) c, and total protein amount (total fluorescence intensity on cell area) $a = cv$ together with cell lineage trees, and calculated $\bar{\lambda}_\tau$, $\bar{p}_\tau$, and $\bar{c}_\tau$ for each cell lineage according to the definitions in Eq. 14-16.

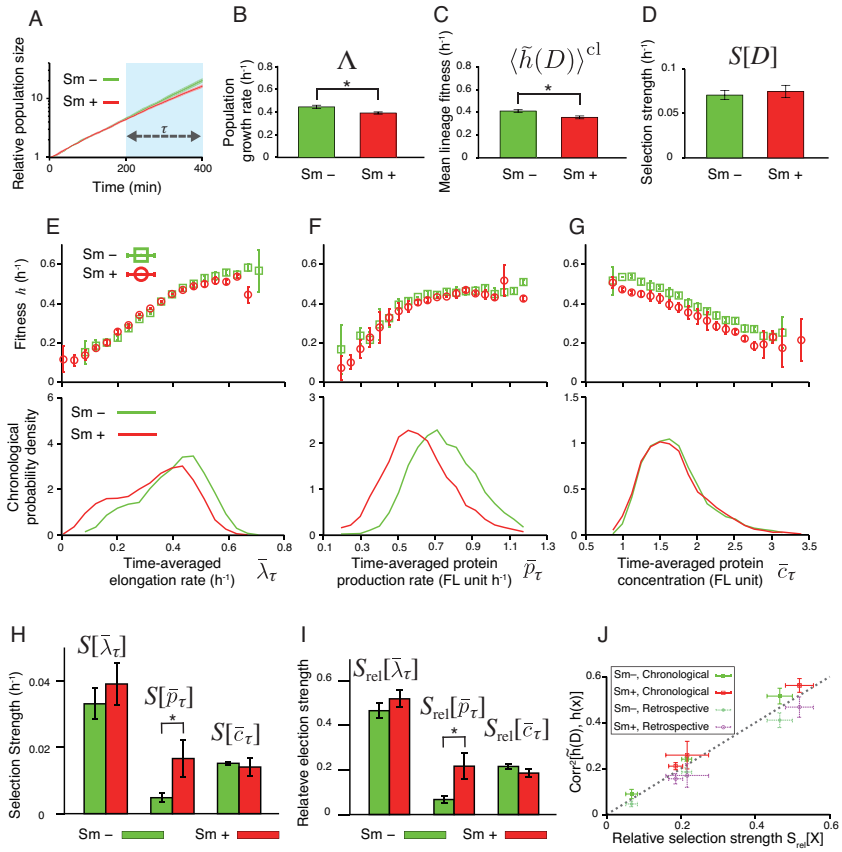

Fig 4. Fitness landscapes and selection strength measured for *E. coli* phenotypes. A. Population growth curves. Green curve is for Sm− condition, and red for Sm+ condition (the color correspondence is the same for all the following panels). Relative population size on Y-axis is the number of cells at each time point normalized by the number of cells at $t = 0$ min. The error bars are the standard deviations of three independent experiments, which is also true for all the error bars in the following panels. Growth rate difference became apparent only after $t = 200$ min. Hence, we set $t_0 = 200$ min and $t_1 = 400$ min in the following analyses. The results with $t_0 = 0$ min and $t_1 = 200$ min are shown in Fig 2 in *Supporting Information*. **B-D.** Comparison of population growth rate Λ (B), chronological mean fitness for division count $\langle \tilde{h}(D) \rangle^{\mathrm{cl}}$ (C), and selection strength for division count $S[D]$ (D), between Sm− and Sm+ conditions. p-values by t-test are 0.013, 0.010, and 0.529, respectively ($n = 3$). **E-G.** Fitness landscapes $h(x)$ (upper panels) and chronological distributions $P^{\mathrm{cl}}(x)$ (lower panels) for elongation rate $\bar{\lambda}_\tau$ (E), protein production rate $\bar{p}_\tau$ (F), and protein concentration $\bar{c}_\tau$ (G). The fitness landscapes for elongation rate and protein production rate were barely distinguishable between Sm− and Sm+ conditions, whereas that for protein concentration shows a slight downshift in Sm+ condition. In contrast, shift of chronological distributions was observed for elongation rate and protein production rate, but not for protein concentration. **H.** Selection strengths. We compared selection strengths $\bar{\lambda}_\tau$, $\bar{p}_\tau$, and $\bar{c}_\tau$ between Sm− and Sm+ conditions, finding a statistically significant difference only for $\bar{p}_\tau$ ($p < 0.05$). The p-values are 0.34 for $\bar{\lambda}_\tau$, 0.044 for $\bar{p}_\tau$, and 0.58 for $\bar{c}_\tau$, respectively ($n = 3$). **I.** Relative selection strengths. Again, the difference is statistically significant only for $\bar{p}_\tau$ ($p < 0.05$). The p-values are 0.21 for $\bar{\lambda}_\tau$, 0.024 for $\bar{p}_\tau$, and 0.14 for $\bar{c}_\tau$, respectively ($n = 3$). **J.** Relationship between relative selection strength and squared correlation coefficient between $\tilde{h}(D)$ and $h(x)$, where $x = \bar{\lambda}_\tau$, $\bar{p}_\tau$, or $\bar{c}_\tau$. The correlation coefficients were evaluated by both chronological and retrospective probabilities.

Materials and Methods

Simulation

We simulated clonal cell proliferation processes using a custom C program. We determined phenotypic state $y_{t+\Delta t}$ by randomly sampling the value of $\ln y_{t+\Delta t}$ from the normal distribution with mean $\mu + e^{-\gamma\Delta t}(\ln y_t - \mu)$ and variance $\sigma^2\left(1 - e^{-2\gamma\Delta t}\right)$ assuming that the transition of $\ln y_t$ follows the Ornstein-Uhlenbeck process. We set $\Delta t = 5$ min, $\mu = -0.5\ln(1.09)$, $\sigma^2 = \ln(1.09)$, and $\gamma = (-0.6\ln r_g)$ h^{-1} with $r_g = 0.8$. In this setting, y_t follows the log-normal distribution with mean 1.0 and standard deviation 0.3 in the stationary state without selection (i.e. Hill coefficient $n = 0$). We assumed that cells divide with the probability of $f(y_t)\Delta t$ with $f_{\max} = 1.2$ h^{-1} at each time point, and the initial states of two daguther cells ($y_{t+\Delta t}$) were determined independently of each other from the last state (y_t) of their mother cell. Without selection, the division rate is $f_0 = f_{\max}/2 = 0.6$ h^{-1} and thereby the mean interdivision time along a lineage is $f_0^{-1} = 0.6^{-1}$ h^{-1}. Without selection, since the normalized autocorrelation function of $\ln y_t$ at stationary sate is $\phi(\tau) = e^{-\gamma\tau}$, $r_g = e^{-\gamma/f_0}$ is the autocorrelation of $\ln y_t$ after a single generation. Fitness landscapes of $\overline{y}_\tau$ with faster fluctuation conditions ($r_g = 0.5$ and 0.2) were shown in Fig S1 in *Supporting Information.* We produced a dataset that contains 100 lineage trees (i.e. $N(t_0) = 100$ cells) with the length of $\tau = 250$ min in each condition, which is comparable to the data size of the real experiments (Table S1 in *Supporting Information*). For each condition, we repeated the simulation 10 times, and the average and standard deviation were shown in Fig 2 and in Fig S1 in in *Supporting Information.*

Cell strain and culture conditions

We used F3 and F3/pTN001 *E. coli* strains in the experiment. F3 is a W3110 derivative strain in which three genes (*fliC*, *fimA*, and *flu*) are deleted. pTN001 is a low copy plasmid constructed from pMW118 (Nippon Gene, Co., LTD), into which we inserted PLlacO-1 promoter [27], *venus-yfp* [26], and sm^R as shown in Fig 3A. *venus-yfp* and sm^R genes were cloned from Venus/pCS2 (gift from A. Miyawaki at RIKEN, JAPAN) and pKP2375 (gift from Dr. H. Niki at National Institute of Genetics, JAPAN), respectively. We cultured the cells in M9 minimal medium (M9 minimal salt (Difco) + 2 mM $MgSO_4$ (Wako) + 0.1 mM $CaCl_2$ (Wako) + 0.2% glucose (Wako)) at 37°C. 0.1 mM Isopropyl β-D-1 thiogalactopyranoside (IPTG) (Wako) was added to the culture of F3/pTN001 to induce Venus-YFP and Sm^R. For single-cell time-lapse experiments, we solidified M9 medium with 1.5% (w/v) agarose (Gene Pure Agarose, BM Bio), and approximately 5 mm (W)×8 mm (D)×5 mm (H) piece of M9 agarose gel was mounted onto cell suspension on a glass-bottom dish (IWAKI). For Sm+ condition, we added 200 µg/mL streptomycin when solidifying M9 agarose gel.

Determination of MIC

An overnight culture of F3 or F3/pTN001 in M9 medium at 37°C from glycerol stock was diluted ×100 into 2-ml fresh M9 medium and cultured for three hours at 37°C. 100 µl exponential phase culture was mixed with 100 µl fresh M9 medium containing streptomycin in a 96-well plate. We prepared 10 different conditions of streptomycin concentration for each strain with the concentration increased in two-fold stepwise. The optical density of the cell cultures after mix was ca. 0.05 at 600 nm. The cell cultures in a 96-well plate were incubated

by shaking at 37°C for 20 hours. We determined the MICs of F3 and F3/pTN001 with a microtiter plate (FilterMax F5, Molecular Devices) by absorbance at 595 nm.

Time-lapse microscopy

To prepare a sample for time-lapse microscopy, we first cultured F3/pTN001 cells from glycerol stock in M9 medium at 37°C by shaking overnight. Next, we diluted the overnight culture ×100 in 2 ml fresh M9 medium, and cultured it for another three hours at 37°C by shaking. We adjusted the OD_{600} of the culture to 0.05, and 1 µl of the diluted culture was spread on a 35-mm (ϕ) glass-bottom dish (IWAKI) by placing M9 agarose pad onto the cell suspension. To avoid drying the M9 agarose pad, water droplets (total 200 µl) were placed around the internal edge of the dish. The dish was sealed by parafilm to minimize water evaporation. Fluorescent time-lapse images were acquired every 5 minutes with Nikon Ti-E microscope equipped with a thermostat chamber (TIZHB, Tokai Hit), 100x oil immersion objective (Plan Apo λ, N.A. 1.45, Nikon), cooled CCD camera (ORCA-R2, Hamamatsu Photonics), and LED excitation light source (DC2100, Thorlabs). The temperature around the dish was maintained at 37°C. The microscope was controlled by micromanager (https://micro-manager.org/).

Analysis

Time-lapse images were analyzed with a custom macro of ImageJ (http://imagej.nih.gov/ij/). This macro produces the results file, which contains the information of mean fluorescence intensity, cell size (area), and geneaological position of individual cells. We analyzed the results file with a custom C program.

To evaluate fitness landscapes and selection strengths both in the simulation and the experiments, we determined the bin width based on the interquartile range of each phenotypic state (Fig S3 and S4 in *Supporting Information*). The details are explained in *Supporting Information*.

Acknowledgments

This work was supported by JSPS KAKENHI Grant Number 25711008, 15KT0075, 15H05746 (YW); NIH Grant Number R01-GM-097356 (EK); and Platform for Dynamic Approaches to Living System from MEXT and AMED, Japan (YW). TN was supported by Grant-in-Aid for JSPS Fellows (14J01376). We thank Reiko Okura and Sayo Akiyoshi for technical assistance, Atsushi Miyawaki for providing Venus/pCS2 plasmid, Hironori Niki for providing pKP2375 plasmid, Ippei Inoue for the technical advice on *E. coli* strain and plasmid construction, and members of Wakamoto lab for in-depth discussions.

References

[1] Sato K, Kaneko K. On the distribution of state values of reproducing cells. Phys Biol. 2006;3(1):74–82. doi:10.1088/1478-3975/3/1/008.

[2] Tănase-Nicola S, Wolde PT. Regulatory control and the costs and benefits of biochemical noise. PLoS Comput Biol. 2008;4(8):1–13. doi:10.1371/journal.pcbi.1000125.

[3] Mora T, Walczak AM. Effect of Phenotypic Selection on Stochastic Gene Expression. J Phys Chem B. 2013;doi:10.1021/jp403231f.

[4] Rivoire O, Leibler S. A model for the generation and transmission of variations in evolution. Proc Natl Acad Sci. 2014;111(19):E1940–E1949. doi:10.1073/pnas.1323901111.

[5] Balázsi G, van Oudenaarden A, Collins J. Cellular Decision Making and Biological Noise: From Microbes to Mammals. Cell. 2011;144(6):910–925. doi:10.1016/j.cell.2011.01.030.

[6] Ackermann M. A functional perspective on phenotypic heterogeneity in microorganisms. Nat Rev Microbiol. 2015;13(8):497–508. doi:10.1038/nrmicro3491.

[7] Balaban NQ, Merrin J, Chait R, Kowalik L, Leibler S. Bacterial persistence as a phenotypic switch. Science. 2004;305(5690):1622–5. doi:10.1126/science.1099390.

[8] Wakamoto Y, Dhar N, Chait R, Schneider K, Signorino-Gelo F, Leibler S, et al. Dynamic Persistence of Antibiotic-Stressed Mycobacteria. Science (80-). 2013;339(6115):91–95. doi:10.1126/science.1229858.

[9] Ackermann M, Stecher B, Freed NE, Songhet P, Hardt WD, Doebeli M. Self-destructive cooperation mediated by phenotypic noise. Nature. 2008;454(7207):987–990. doi:10.1038/nature07067.

[10] Süel GM, Kulkarni RP, Dworkin J, Garcia-Ojalvo J, Elowitz MB. Tunability and noise dependence in differentiation dynamics. Science. 2007;315(5819):1716–9. doi:10.1126/science.1137455.

[11] Fisher RA. The Genetical Theory of Natural Selection. Clarendon; 1930.

[12] Elena SF, Lenski RE. Microbial genetics: Evolution experiments with microorganisms: the dynamics and genetic bases of adaptation. Nat Rev Genet. 2003;4(6):457–469. doi:10.1038/nrg1088.

[13] Hashimoto M, Nozoe T, Nakaoka H, Okura R, Akiyoshi S, Kaneko K, et al. Noise-driven growth rate gain in clonal cellular populations. Proc Natl Acad Sci. 2016;113(12):3251–3256. doi:10.1073/pnas.1519412113.

[14] Lambert G, Kussell E. Quantifying Selective Pressures Driving Bacterial Evolution Using Lineage Analysis. Phys Rev X. 2015;5:1–10. doi:10.1103/PhysRevX.5.011016.

[15] Ni M, Decrulle AL, Fontaine F, Demarez A, Taddei F, Lindner AB. Pre-disposition and epigenetics govern variation in bacterial survival upon stress. PLoS Genet. 2012;8(12):e1003148. doi:10.1371/journal.pgen.1003148.

[16] Stewart EJ, Madden R, Paul G, Taddei F. Aging and death in an organism that reproduces by morphologically symmetric division. PLoS Biol. 2005;3(2):e45. doi:10.1371/journal.pbio.0030045.

[17] Murray JI, Bao Z, Boyle TJ, Boeck ME, Mericle BL, Nicholas TJ, et al. Automated analysis of embryonic gene expression with cellular resolution in C. elegans. Nat Meth. 2008;5(8):703–709.

[18] Xiong F, Ma W, Hiscock T, Mosaliganti K, Tentner A, Brakke K, et al. Interplay of Cell Shape and Division Orientation Promotes Robust Morphogenesis of Developing Epithelia. Cell. 2014;159(2):415–427. doi:10.1016/j.cell.2014.09.007.

[19] Leibler S, Kussell E. Individual histories and selection in heterogeneous populations. Proc Natl Acad Sci U S A. 2010;107(29):13183–8. doi:10.1073/pnas.0912538107.

[20] Wakamoto Y, Grosberg AY, Kussell E. Optimal lineage principle for age-structured populations. Evolution (N Y). 2011;66(1):115–134. doi:10.1111/j.1558-5646.2011.01418.x.

[21] Kobayashi TJ, Sughiyama Y. Fluctuation Relations of Fitness and Information in Population Dynamics. Phys Rev Lett. 2015;115(23):238102. doi:10.1103/PhysRevLett.115.238102.

[22] Jeffreys H. Theory of Probability. 2nd ed. Oxford University Press; 1948.

[23] Kullback S, Leibler R. On Information and Sufficiency. Ann Math Stat. 1951;.

[24] Frank SA. Natural selection. V. How to read the fundamental equations of evolutionary change in terms of information theory. J Evol Biol. 2012;25(12):2377–96. doi:10.1111/jeb.12010.

[25] Onogi T, Miki T, Hiraga S. Behavior of Sister Copies of Mini-F Plasmid after Synchronized Plasmid Replication in Escherichia coli Cells. J Bacteriol. 2002;184(11):3142–3145. doi:10.1128/JB.184.11.3142.

[26] Nagai T, Ibata K, Park ES, Kubota M, Mikoshiba K, Miyawaki A. A variant of yellow fluorescent protein with fast and efficient maturation for cell-biological applications. Nat Biotechnol. 2002;20(1):87–90. doi:10.1038/nbt0102-87.

[27] Lutz R, Bujard H. Independent and tight regulation of transcriptional units in Escherichia coli via the LacR / O , the TetR / O and AraC / I 1 -I 2 regulatory elements. Nucleic Acids Res. 1997;25(6):1203–1210.

[28] Hayes JD, Wolft CR. Molecular mechanisms of drug resistance. Biochem J. 1990;272(2):281–295.

[29] Kawabe H, Tanaka T, Mitsuhashi S. Streptomycin and Spectinomycin Resistance Mediated by Plasmids. Antimicrob Agents Chemother. 1978;13(6):1031–1035.

[30] Lande R, Arnold SJ. The Measurement of Selection on Correlated Characters. Evolution (N Y). 1983;.

[31] Geyer CJ, Shaw RG. Commentary on Lande-Arnold Analysis. Minneapolis, MN: School of Statistics/University of Minnesota; 2008. 670.

[32] Shaw RG, Geyer CJ. Inferring fitness landscapes. Evolution. 2010;64(9):2510–20. doi:10.1111/j.1558-5646.2010.01010.x.

[33] Lange C, Calegari F. Cdks and cyclins link G1 length and differentiation of embryonic, neural and hematopoietic stem cells. Cell Cycle. 2010;9(10):1893–1900. doi:10.4161/cc.9.10.11598.

[34] Keller PJ, Schmidt AD, Wittbrodt J, Stelzer EHK. Reconstruction of zebrafish early embryonic development by scanned light sheet microscopy. Science. 2008;322(5904):1065–9. doi:10.1126/science.1162493.

[35] Pantazis P, Supatto W. Advances in whole-embryo imaging: a quantitative transition is underway. Nat Rev Mol Cell Biol. 2014;15(5):327–339.

[36] Worobey M, Han GZ, Rambaut A. A synchronized global sweep of the internal genes of modern avian influenza virus. Nature. 2014;508(7495):254–7. doi:10.1038/nature13016.

[37] Fraser C, Lythgoe K, Leventhal GE, Shirreff G, Hollingsworth TD, Alizon S, et al. Virulence and pathogenesis of HIV-1 infection: an evolutionary perspective. Science. 2014;343(6177):1243727. doi:10.1126/science.1243727.

[38] Greenbaum BD, Ghedin E. Viral evolution: beyond drift and shift. Curr Opin Microbiol. 2015;26:109–115. doi:10.1016/j.mib.2015.06.015.

[39] Luksza M, Lässig M. A predictive fitness model for influenza. Nature. 2014;507(7490):57–61. doi:10.1038/nature13087.

[40] Neher RA, Russell CA, Shraiman BI. Predicting evolution from the shape of genealogical trees. Elife. 2014;3:e03568. doi:10.7554/eLife.03568.